

Supporting Online Material for

Balanced inhibition and excitation drives spike activity

in spinal half-centers

Rune W. Berg¹, Aidas Alaburda², & Jørn Hounsgaard^{1*}

¹Department of Neuroscience and Pharmacology, Panum Institute, University of
Copenhagen DK 2200 Copenhagen N, Denmark.

²Department of Biochemistry and Biophysics, Faculty of Natural Sciences, Vilnius
University, Ciurlionio 21/27, 03101 Vilnius, Lithuania

*To whom the correspondence should be addressed. Email: j.hounsgaard@mfi.ku.dk

Published dd.mm.yyyy in Science

This PDF file includes:

Materials and Methods

5 Figures

References

MATERIALS AND METHODS

Integrated preparation. Red-eared turtles (*Trachemys scripta elegans*) were placed on crushed ice for 2 hr to ensure hypothermic anesthesia (1). Animals were killed by decapitation and blood substituted by perfusion with a Ringer solution containing (mM): 120 NaCl; 5 KCl; 15 NaHCO₃; 2 MgCl₂; 3 CaCl₂; and 20 glucose, saturated with 98% O₂ and 2% CO₂ to obtain pH 7.6. The carapace containing the D4-D10 spinal cord segments was isolated by transverse cuts and removed from the animal (2-3). The surgical procedures complied with Danish legislation and were approved by the controlling body under the Ministry of Justice.

Recordings. Intracellular recordings in current-clamp mode were performed with an Axoclamp-2A amplifier. In most experiments glass pipettes were filled with a mixture of 0.9 M potassium acetate and 0.1 M KCl. In some experiments electrodes contained a mixture of 0.9 M cesium acetate and 0.1 M CsCl to reduce potassium conductance and QX 314 (2 (triethylamino)-N-(2,6- dimethylphenyl) acetamide, 0.2M final concentration)) to block action potentials in the cell recorded from.

Intracellular recordings were obtained from neurons in segment D10. Recordings were accepted if neurons had a stable membrane potential more negative than -50 mV. Data were sampled at 20 kHz with a 12-bit analog-to-digital converter, displayed by means of Axoscope and Clampex software, and stored on a hard disk for later analysis.

Hip Flexor nerve activity was recorded with a differential amplifier Iso-DAM8 using a suction pipette. The bandwidth was 100 Hz – 1 kHz.

Stimulation. Mechanical stimulation was performed with the fire polished tip of a bent glass rod mounted to the membrane of a loudspeaker. The duration, frequency, and amplitude of the stimulus were controlled with a function generator (3).

Data analysis. Estimation of synaptic conductances. All calculations were performed in Matlab. The mean total conductance (G_{total}) (Fig. 1D and 4) was estimated by applying Ohm's law on the membrane potential, V_m , during consecutive scratch episodes recorded

at different levels of constant current injections, I_{inj} . G_{total} was estimated by the slope of a line fitted to the VI-plot at each point in time (4-6). The overall alignment of trial- V_m in time was triggered by the onset of the mechanical stimulus and fine-tuned by the maximal cross-covariance of full-way rectified and smoothed nerve activity. The mean inhibitory and excitatory synaptic conductances were estimated from (4-6)

$$G_i(t) = \frac{G_{Leak} \cdot (E_{Leak} - E_e) + G_{total}(t) \cdot (E_e - V_m(t)) - I_{inj}}{E_e - E_i} \quad (\text{Eq. 1})$$

$$G_e(t) = G_{total}(t) - G_i(t) - G_{Leak} \quad (\text{Eq. 2})$$

where G_{Leak} is the constant leak conductance and E_{Leak} is the leak reversal potential (set to -60 mV). Equation 1 and 2 were rearranged from the principal equation (4-6) following from Ohm's law and Kirchhoff's current law in a one-compartment scheme:

$$C_m \frac{dV_m}{dt} = G_{Leak} \cdot (E_{Leak} - V_m(t)) + G_i(t) \cdot (E_i - V_m(t)) + G_e(t) \cdot (E_e - V_m(t)) - I_{inj} = 0$$

ignoring rapid changes in V_m (4-6). The assumption that contributions to the conductance are either constant or from synaptic sources gives (4-6):

$$G_{total}(t) = G_e(t) + G_i(t) + G_{Leak}$$

Assumptions were verified by intracellular application of QX-314 and Cs^+ (6), and justified by the fact that synaptic intensity (spectral power) was correlated with total conductance (Fig. 4). The estimates of G_{total} , G_i and G_e did not depend on the level of hyperpolarizing holding current, i.e. they were unaffected by voltage sensitive conductances. We also note that the phase relation between nerve activity and the depolarizing waves in motoneurons was unaffected by holding current. E_e is the reversal potential for the excitatory drive and set to $E_e = 0$ and E_i is the inhibitory drive. E_i was estimated in each cell by varying current injection and visually inspecting of the potential that reverses spontaneous IPSPs (usually $E_i = -65$ mV). G_{Leak} was estimated in each trial

as 80% of the total conductance during quiescence ($G_{\text{Leak}} = 40\text{-}80$ nS). Note that the exact choice of E_e , E_i , E_{Leak} and G_{Leak} had no effect on the coherence estimates and thus the conclusions of the present study.

The estimates of G_{Leak} , G_i and G_e rely on the simplifying assumption that leak, inhibition and excitation is homogeneously distributed over the soma-dendritic surface and that each of these conductances can be represented by a single reversal potential (one-compartment model).

Coherence between Inhibition and excitation

The increase in synaptic conductances (Fig. 1F) was calculated as

$$\Delta G = \frac{G - G_{\min}}{\max(G - G_{\min})}$$

The sole purpose of this metric was illustration, since its informational content is equivalent to the complex-valued coherence, which was easier to quantify for the population (cf. Fig. 1F and 1G). Thus, the quantification the complex-valued coherence between the inhibition and excitation was calculated as

$$coherence = \frac{\langle \overline{G_e} \cdot \overline{G_i}^* \rangle}{\sqrt{\langle |\overline{G_e}|^2 \rangle \langle |\overline{G_i}|^2 \rangle}}$$

Where $\overline{G_e} \cdot \overline{G_i}^*$ denotes the cross-power spectrum between the excitatory and inhibitory conductance and $|\overline{G}|^2$ denotes the respective power spectrum. The brackets $\langle \dots \rangle$ denotes average over estimates for individual trials and across trials (7-9). The single trial power spectra and cross-spectra were estimated as an average over $K = 4$ independent estimates using the multi-taper method (7-9). For each trial the coherence at the peak frequency of the rectified and smoothed nerve recording was plotted as a vector in the complex plane (Fig. 1G-I) as a way to compare the phase and magnitude across the whole population and assessing significance (7). Confidence limits for the magnitude of the coherence were estimated as (9)

$$|c| = \sqrt{1 - \frac{1}{p^{NK-1}}}$$

where $p = 0.05$ for the 95 % confidence limit, N is the number of trials. For a single trial the radius of confidence is 0.79 (outer gray circle, Fig. 1G-I). The largest radius of confidence across cells was shown for illustration (gray circles in Fig. 1H-I) and the red arrows are the averages also for illustration of trends across populations.

Data analysis. Subthreshold analysis. Negative current was injected so no action potentials occurred even during the scratch activity. The power spectrum of V_m was estimated as described above ($K = 3$) for windows of 500 ms length at each 30 ms of the high-pass filtered V_m (sampling frequency = 10 KHz, cut-off = 8 Hz).

Data analysis. Rastograms and Fano factor. The rastograms were produced across trials by triggering on the peak of nerve activity, for each cycle in the scratch episode (Fig. 1 AB). The Fano factor was calculated for each cycle as the variance divided by the mean number of spikes per cycle (10-11) (Fig S5) which is a measure of how variable the number of spikes of each cycle is from trial to trial. The advantage of the Fano factor is its insensitive to non-stationarity, opposed to the complementary common measure Coefficient of variation (CV) of the ISI defined as the standard deviation of the ISI divided by the mean of the ISI. See Fig S5 for more information.

Drugs: Receptor antagonists were added to the superfusion solution: 6-Cyano-7-nitroquinoxaline-2,3-dione (CNQX, 25 μ M) and DL-2-amino-5-phosphonopentanoic acid (DL-AP5, 50 μ M); strychnine, (10 μ M). Strychnine (10 μ M). QX 314 (2 (triethylamino)-N-(2,6- dimethylphenyl) acetamide(0.2 M)) was added to pipette solution to block action potentials.

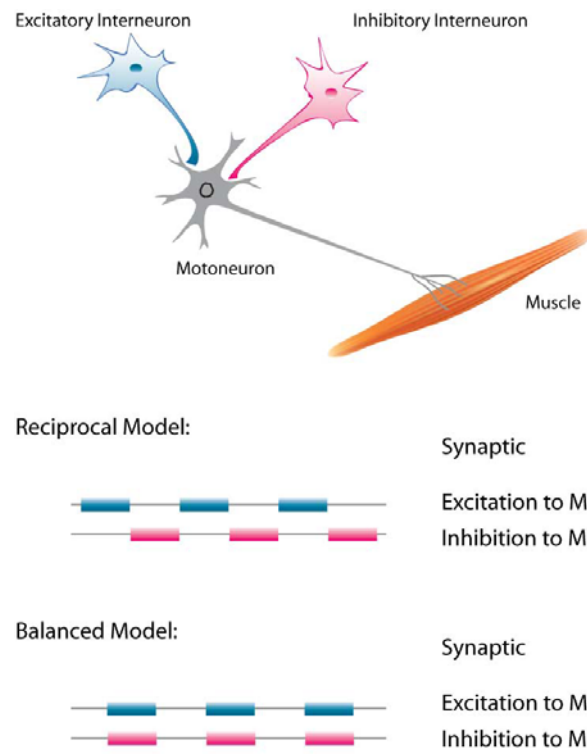


Figure S1. Schematics. During scratching motoneurons are thought to be excited and inhibited in alternation (Reciprocal Model). In contrast, our experiments show that synaptic inhibition and excitation alternate in phase during scratching (Balanced Model)

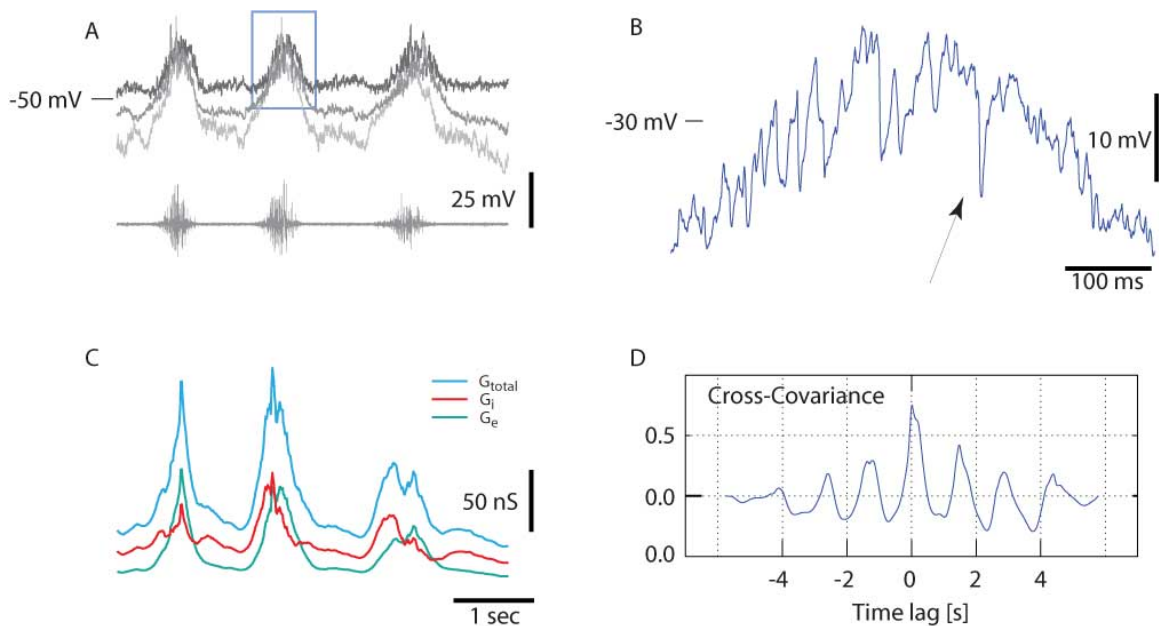


Figure S2. Estimates of total conductance, inhibitory conductance and excitatory conductance in the absence of spikes and with reduced K^+ conductance (QX314 and Cs^+ in recording electrode)

A. V_m recorded during scratch episodes at 3 levels of holding current (upper records, -1.5, -1.0, and -0.5 nA), aligned with nerve recording (lower record). **B.** Blow-up of synaptic fluctuations in trace from framed section in **A**. (Note hyperpolarizing transients). **C.** Conductances estimated from **A**. The average excitatory and inhibitory conductance co-varies with total conductance. **D.** Cross-covariance between inhibitory and excitatory traces in **C**. The correlation is highly significant and centered around zero.

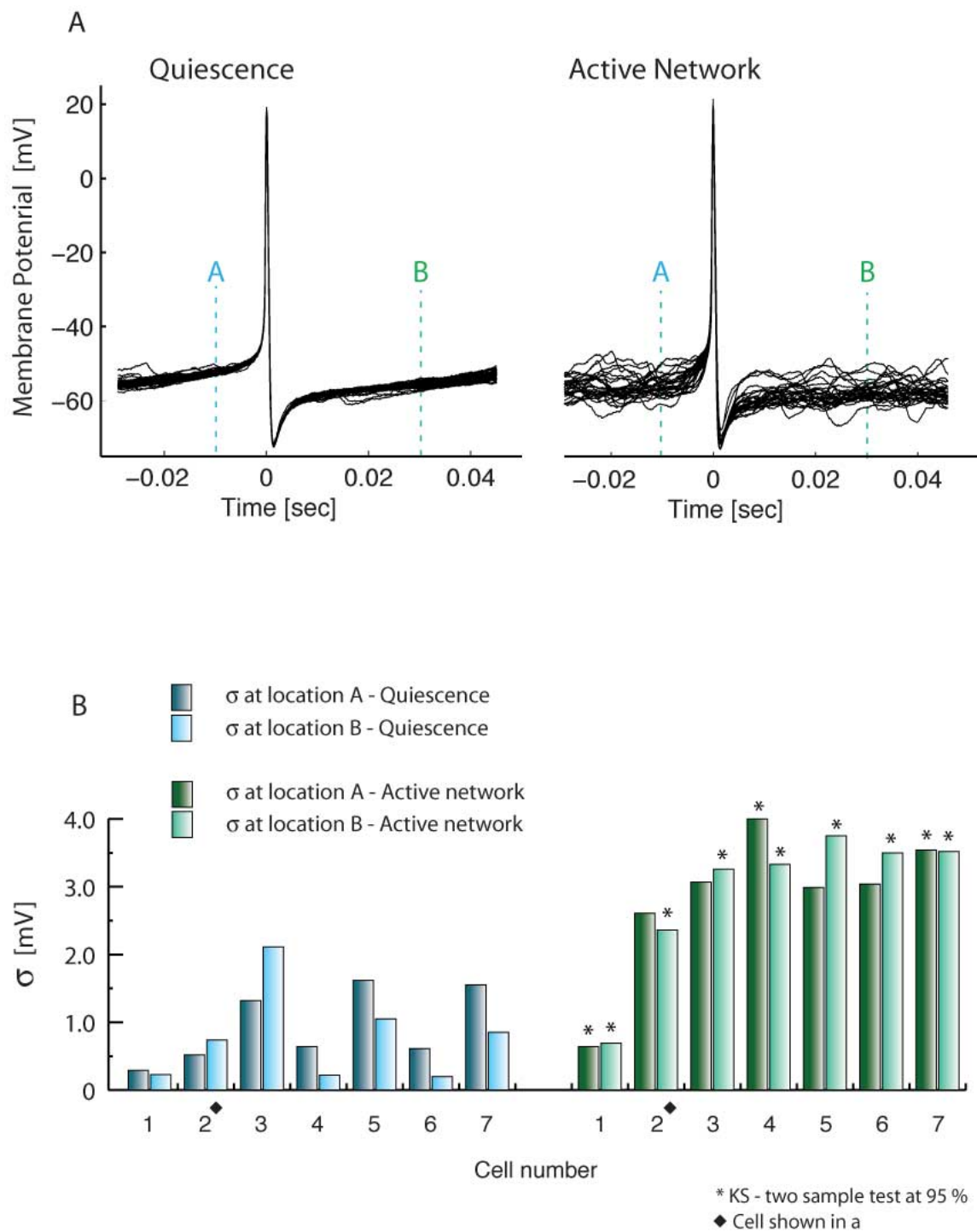


Figure S3. Interspike voltage trajectory in quiescence and during network activity.

A. Superimposed spikes during quiescence, i.e. little synaptic input, and during network activity. **B.** The sigma of the membrane potential across trials at location A and B, in **A**, for all cells tested ($n = 7$).

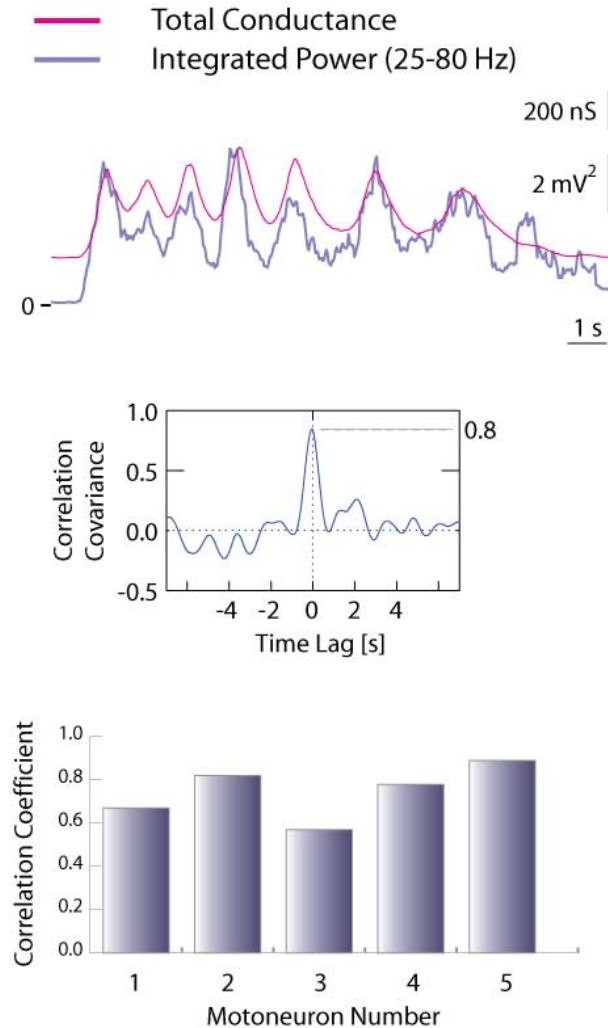


Figure S4. Correlation between total conductance and integrated spectral power.

Top: Total conductance (pink) plotted with the 25-80 Hz integrated power of the membrane potential in a 300 ms sliding window. Middle: Correlation covariance function between total conductance and integrated power from top, demonstrates clear significant correlation between total conductance and synaptic bombardment. Bottom: The average correlation coefficient (measured at the broken line in middle panel) across all cells tested ($n = 5$, $n = 14$ trials total).

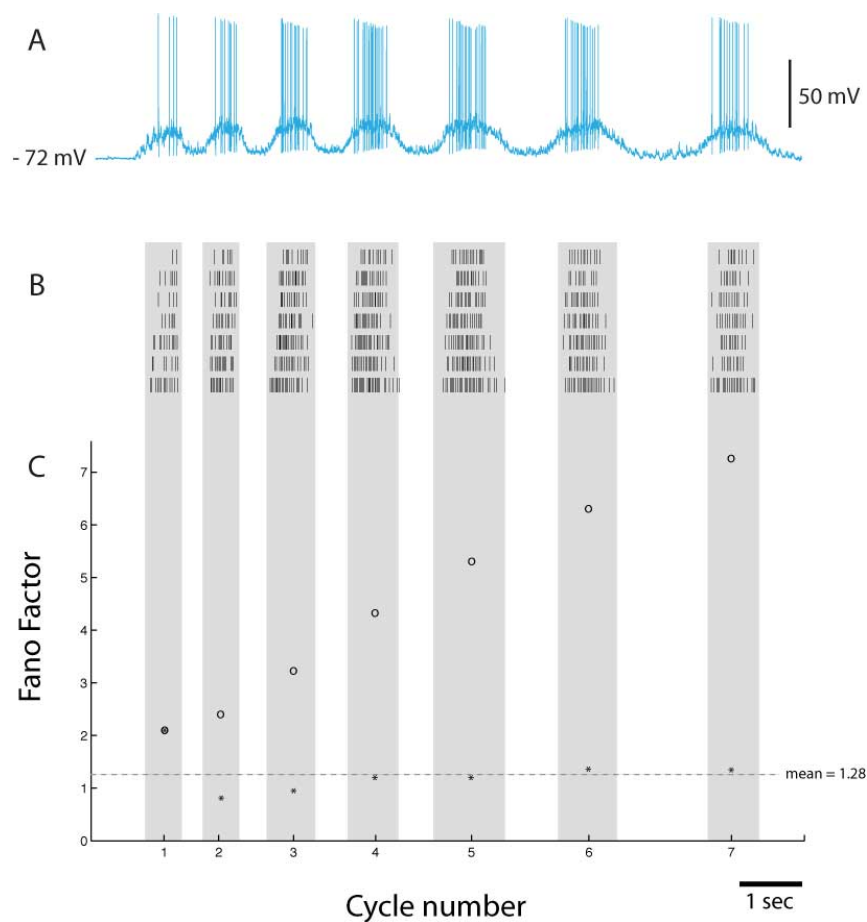


Figure S5. High variability across trials: Fano factor. **A.** Intracellular recording from motoneuron during one of seven consecutive scratch episodes. **B.** Raster-plot of spike timing in 7 consecutive scratch episodes (episode from **A** included) shows irregular spiking during depolarizing waves within and across scratch episodes. **C.** Counting spikes within a fixed time window is a measure of the variability of synaptic input. The Fano factor is the fraction of variability in spike count over the mean spike count across trials. “*” is the Fano factor for individual cycles, “o” is the accumulated Fano factor for cycles. The steady increase in the accumulated Fano factor suggests long range correlations on a time scale exceeding single cycles (10-11). The average single cycle Fano factor is close to 1, which is the expected value for a poisson process (1-2). Table of Fano factors for single cycles averaged over cycles and single scratch episodes in 10 motoneurons.

Supporting References

- 1 Melby ECJ, Altman NH “Handbook of laboratory animal science” Cleveland: CRC (1974)
2. Alaburda A & Hounsgaard J Metabotropic modulation of motoneurons by scratch-like spinal network activity. *J Neurosci.* 23(25):8625-8629 (2003)
3. Alaburda A, Russo R, MacAulay N, and Hounsgaard J Periodic High-Conductance States in Spinal Neurons during Scratch-Like Network Activity in Adult Turtles . *J. Neurosci.* 25 6316-6321(2005)
- 4 J. S. Anderson, M. Carandini, D. Ferster, *J. Neurophysiol.* **84**, 909 (2000)
5. Y. Shu, A. Hasenstaub, D.A. McCormick, *Nature* **423**, 288 (2003)
6. J. Marino, J. Schummers, D.C. Lyon, L. Schwabe, O. Beck, P. Wiesing, K. Obermayer, M. Sur, *Nat. Neurosci.* **8**, 194 (2005).
7. Berg RW, Whitmer D, Kleinfeld D, “Exploratory whisking by rat is not phase locked to the hippocampal theta rhythm” *J. Neurosci.* 26(24): 6518-6522. (2006)
8. Persival DB, Walden AT, Spectral analysis for physical application: multitaper and conventional univariate techniques” chapter 7, Cambridge, UK: Cambridge UP. (1993)
9. Jarvis MR, Mitra PP “Sampling properties of the spectrum and coherency of sequences of action potentials”, *Neural computat.* 13: 717-749, (2001)
- 10 Rieke F, Warland D, Ruyter van Stevenick Rd, Bialek W “Spikes – Exploring the neural code” Chapter 2. MIT press, Cambridge Massachusetts. (1997)
- 11 Gabbiani F, Koch C, Book chapter: “Principles of spike train analysis” in “Methods in neuronal modeling” 2nd edition MIT press 2001